Food Chemistry: X 15 (2022) 100402

Contents lists available at ScienceDirect

Food Chemistry: X

journal homepage: www.sciencedirect.com/journal/food-chemistry-x

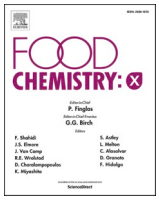

Characterization of coacervation behavior between whey protein isolate and propylene glycol alginate: A morphology, spectroscopy, and thermodynamics study

Chunyu Xi, Zhengwei Sun, Xing Chen, Xuan Ding, Tiehua Zhang *

College of Food Science and Engineering, Jilin University, Changchun 130062, PR China

ARTICLE INFO

Keywords:
Whey protein isolate
Propylene glycol alginate
Interaction mechanism
Isothermal titration calorimetry

ABSTRACT

The interactions between whey protein isolate (WPI) and propylene glycol alginate (PGA) were investigated as a function of pH and the mass ratio. The results showed that WPI and PGA formed a soluble and uniform complex at a mass ratio of 2:1 and pH 4.0 through forces such as electrostatic attraction and hydrogen bonding. Isothermal titration calorimetry confirmed that the contribution of positive enthalpy (ΔH) and entropy (ΔS) were the beneficial indicator in the process of combining WPI and PGA under the same mass ratio but different pH. Fourier transform infrared spectroscopy, fluorescence spectroscopy and circular dichroism confirmed that hydrogen bonding was also one of the interaction forces in addition to electrostatic interactions between WPI-PGA complex. The freeze-dried WPI-PGA complex showed the same amorphous structure as WPI. These formed WPI-PGA complexes provided insights for interaction mechanism of proteins and polysaccharides as well as a theoretical basis for the food industry.

1. Introduction

Proteins and polysaccharides are of considerable interest in the food industry due to the fact of their dietary practical properties (Wu, Lin, Singh, & Ye, 2020). In addition, the structural and functional characteristics of proteins can be effectively improved by the interactions between proteins and polysaccharides (Azeredo & Waldron, 2016) by processes such as solubility, foaming, emulsifying and by exploiting their thermal stability (Xiong et al., 2016), and antioxidant properties (Guo, et al., 2021), and these interactions can be broadly applied in food, medicine, and beauty industries. In preceding studies, the interactions mechanism between proteins and polysaccharides (Schmitt & Turgeon, 2011); in general fashioned by way of the enchantment of two oppositely charged biopolymers. The factors influencing the properties of complexes were identified as being the mass ratio of the two biopolymers, pH, and ionic strength (Feng, Sun, Wang, Sun, & Shao, 2020; Samanta & Ganesan, 2018). In this respect, the coacervation behavior between proteins and polysaccharides through different influencing factors has become a topic of research interest (Yang, et al., 2020).

Whey protein isolate (WPI) is broadly used as a raw material for emulsifiers and nutritional carriers in the ready meal industry, due to its precise emulsification, gelation, and foaming properties as well as often providing food with a satisfactory appearance, taste, texture, and rheology (Wei et al., 2021). However, the industrial application of WPI is constrained due to the fact of decreased solubility, emulsifying stability, and even coagulation underneath sure processing stipulations (Kuhn, Drummond e Silva, Netto, & da Cunha, 2014). Previous research have proved that the interactions between WPI and polysaccharides efficaciously expanded the emulsifying properties and rheological properties of WPI, ensured the health standards during the preparation process (Wu, Lin, Singh, & Ye, 2020), and it is thus evident that the application values of WPI can be improved through the interactions with polysaccharides. For example, Shang et al. studied the electrostatic interplay between WPI and Flammulina velutipes polysaccharide to enhance the solubility and balance of WPI (Shang, et al., 2021). Doost, A. S., et al. (Doost, Nasrabadi, Kassozi, Dewettinck, Stevens, & Van der Meeren, 2019) studied the formation of a nanocomplex through WPI and almond gum via electrostatic interaction, which provided good emulsion stability; and (Klein, Aserin, Ben Ishai, & Garti, 2010) studied the interaction between WPI and arabic gum when forming a complex that showed good interfacial activities. However, these studies focused only on polysaccharides containing hydrophilic groups, whereas studies on WPI and amphiphilic polysaccharides are limited.

Propylene glycol alginate (PGA) is an anionic hydrophilic

* Corresponding author.
E-mail address: zhangth@jlu.edu.cn (T. Zhang).

https://doi.org/10.1016/j.fochx.2022.100402
Received 19 April 2022; Received in revised form 15 July 2022; Accepted 22 July 2022
Available online 26 July 2022

polysaccharide composed of D-mannuronic acid and L-guluronic acid linked by using 1,4-glycosidic bonds that is generated by an esterification reaction and is mostly used to enhance the functional properties of water-soluble proteins. The propylene glycol group in the molecule is lipophilic and it can bind to hydrophobic groups, and the uronic acid of the molecule has a hydrophilic end (with many hydroxyl organizations and some carboxyl groups) that can be mixed with proteins. PGA has each hydrophilic and lipophilic companies with desirable floor activities. Furthermore, PGA is mostly used to enhance functional properties of water-soluble proteins (Guo, et al., 2021). To the best of our knowledge, the coacervation behavior between WPI and PGA has not been previously reported. Therefore, the study of the electrostatic interactions between WPI and PGA involving the hydrophilic and lipophilic groups leading to an enhancement of the structural and functional properties of WPI is gainful.

The objectives of this study were as follows: (1) to analyze the coacervation behavior between WPI and PGA as features of pH and their mass ratios, and to verify the interaction mechanism between WPI and PGA; (2) to evaluate the thermodynamic characteristics and parameters of the interactions between WPI and PGA using isothermal titration calorimetry (ITC); (3) to investigate the structural characteristics of WPI-PGA complexes using fluorescence spectroscopy, Fourier transform infrared spectroscopy (FTIR), circular dichroism (CD), scanning electron microscopy (SEM), X-ray diffractometry (XRD), and atomic force microscopy (AFM). Such information will provide useful structural features and physicochemical indicators for studying the electrostatic coacervation behavior of WPI and PGA.

2. Materials and methods

2.1. Materials

WPI was once bought from Hilmar (Hilmar 9410, CA, USA), PGA (purity of 98 %) used to be bought from Shanghai Yuanye Bio-Technology Co., ltd. (Shanghai, China). Sodium hydroxide (37 % by way of weight) and hydrochloric acid (37 % with the aid of weight) were obtained from the Beijing Chemical Works (Beijing, China). All other chemical reagents used were analytically pure and required no further purification.

2.2. Preparation of WPI-PGA complex solutions

WPI (0.4 %, w/v) and PGA (0.2 %, w/v) were prepared by dissolving together in deionized water and stirring for 4 h under the action of a magnetic stirrer at 600 rpm to ensure full hydration. The WPI-PGA complex 0.6 % (w/v) was prepared by mixing WPI and PGA stock solution, adjusting to pH of 2.0, 2.5, 3.0, 3.5, 4.0, 4.5, 5.0, 5.5, and 6.0, respectively, with 0.1 M HCl and 0.1 M NaOH, and stirring at 600 rpm for 3 h at a mass ratio of 2:1 (w/w). Some of the samples were refrigerated at 4 ℃ for subsequent property determination, while the others were pre-frozen at −80 ℃ and then lyophilized using an Alphal-2 vacuum freeze dryer (Martin Christ, Germany). Other WPI-PGA complexes 0.6 % (w/v) with mass ratios of 20:1, 10:1, 5:1, 2:1 and 1:1 (w/w), respectively, were also prepared for similar characterization.

2.3. Particle size, PDI and zeta potential measurements

The measurements were conducted using the method of (Shi et al., 2021) but with slight modifications. The mean particle size, PDI and zeta potential of the WPI-PGA complexes were detected using a Malvern Nano ZS Particle Size Analyzer (Malvern Instruments ltd., Worcestershire, UK). Prior to analysis, the different WPI-PGA complexes were diluted with deionized water at a ratio of 1:100 and equilibrated at 25 ℃ for 60 s. Each sample was measured three times and the average value was employed.

2.4. Turbidity measurements

The turbidity (T) of WPI-PGA complexes was measured at 600 nm using a UV spectrophotometer (MOS-500, Bio-logic, Seyssinet-Pariset, France). T was calculated as described by Yadav et al. (2007) but with slight modifications,

$$T = 2.303 \times A \times D/l,$$

where T is turbidity (cm^{-1}), A is absorbance at 600 nm, D is the dilution factor, and l is the path length (cm) of the cuvette.

2.5. Fluorescence

The fluorescence emission spectra of WPI-PGA were measured using an RF = 5301PC fluorescence spectrophotometer (Shimadzu, Japan). The fluorescence spectrum of the WPI-PGA complexes was recorded at an excitation wavelength of 280 nm (exciting tryptophan fluorescence) in the emission wavelength range of 290–450 nm. The concentration of the complex was diluted to 0.1 mg/mL, each sample was measured three times, and the average value was used.

2.6. Circular dichroism (CD)

Both WPI and WPI-PGA were analyzed using a MOS-500 Chirascan Plus (Bio-Logic, France) at the wavelength range of 190–260 nm with a 1 mm path length. The concentration of the complex was diluted to 1 mg/mL, each sample was measured three times, and the average value was taken. Furthermore, the secondary structure content of the WPI in the WPI-PGA complexes with different pH and mass ratio was calculated using Dichroweb: (the online CD website http://dichroweb.cryst.bbk.ac.uk).

2.7. Fourier transform infrared (FTIR)

Two milligrams of WPI and freeze-dried WPI-PGA were mixed with 200 mg of dried potassium bromide and ground under infrared light. The spectra were collected within the wavenumber range of 4000–400 cm^{-1} (resolution 4 cm^{-1}) and averaged over 64 scans. A blank control was used by potassium bromide tablet. The spectrum collection of each sample was repeated three times under the same conditions.

2.8. Isothermal titration calorimetry (ITC)

An isothermal titration calorimeter (Nano-ITC, TA-Instruments, New Castle, Delaware, USA) was used to measure the thermodynamic parameters produced by the titration of the PGA solution (1 μM, 0.234 mg/mL) with the WPI solution (500 μM, 10.8 mg/mL) at different pH (3.5, 4.0, and 4.5). Sample solutions were degassed under vacuum for 20 min. WPI and PGA solutions were placed in a 300 μL reaction cell and a 50 μL syringe, respectively. Each injection was 2.5 μL and lasted 2 s at 350 rpm stirring speed. There was an equilibration time of 250 s between injections, and injections occurred continuously 20 times. A thermal analysis diagram was produced, and the combined isotherms were fitted. The thermodynamic parameters calculated included the affinity constant (K), binding stoichiometry (N), changes in enthalpy (ΔH), and entropy (ΔS).

2.9. X-ray diffractometry (XRD)

An XRD (XRD-6000, Shimadzu, Japan) equipped with a Cu target ceramic X-ray tube with a resolution of 0.0001, an acceleration voltage of 40 kV, a current of 40 mA, a sample scanning range of 5°~60°, and a scanning speed of 0.02°/s was used to analyze the samples. The freeze-dried sample was ground evenly and spread on the sample cell, and the effect of PGA on the crystal structure of WPI was studied and recorded.

2.10. Scanning electron microscope (SEM) meansurments

An SEM (Merlin compact, Zeiss, Germany) was used to observe the microstructure of the samples at a magnification of 1000× at an accelerating voltage of 5.0 kV. The lyophilized samples were coated with a layer of gold metal under high vacuum to avoid charging under electron beam conditions, which could affect the results.

2.11. Statistical analysis

All experiments were repeated three times, and the effects were expressed as means ± standard deviations. Data were evaluated using the one-way evaluation of variance (ANOVA) via the SPSS software program (Version 24.0, SPSS Inc., Chicago, IL, USA), and significant variations were classified as greater than 5 % degrees ($P < 0.05$).

3. Results and discussion

3.1. Effects of pH on the associative coacervation behavior of WPI and PGA

The complex coacervation behavior of proteins and polysaccharides is broadly speaking produced by using electrostatic interaction, which involves the association between oppositely charged biopolymers (Shang, et al., 2021). The zeta potential of WPI increased from −36.1 mV to 34.5 mV as the pH dropped from 6.0 to 2.0, and the isoelectric point of WPI was 4.2 and its associated net charge was zero (Fig. 1A). PGA was consistently negatively charged in this pH range, but it exhibited an increasing trend as the pH dropped from 6.0 to 2.0. The zeta potential of the complexes was intermediate between WPI and PGA, and it improved as the pH dropped.

As shown in Fig. 1B, the solution was once shut to obvious at pH 5.0–6.0. This is due to each WPI, and PGA being negatively charged when found in Fig. 1A, indicating WPI and PGA have been in a co-soluble state. The solution looked grew to be cloudy, however no precipitation happened when the pH dropped to 4.5. The results showed that the electrostatic repulsion of biopolymers with a net negative charge resisted the electrostatic interaction between WPI and PGA. The PGA macromolecules in the system prevented the aggregation of WPI so that no precipitation occurred (Fig. 1A) (Gorji, Gorji, & Mohammadifar, 2014). At pH 4.0, WPI and PGA formed a complex due to electrostatic attraction because the surface of WPI was positively charged. At pH 2.0–3.5, WPI and PGA were attracted to each other due to their opposite charges as the pH further decreased, causing the complex to precipitate. Furthermore, as the positive charge on the surface of WPI increases, the electrostatic interaction increased. The insoluble coacervate reached its maximum at pH 3.0; due to the positively charged WPI, and the negatively charged PGA attracting each other, resulting in a net charge of 0 and forming the largest insoluble biopolymer. A similar phenomenon occurred during the acid titration of a WPI-flaxseed gum complex solution in a previous report (Liu, Shim, Shen, Wang, & Reaney, 2017), the place insoluble coacervates shaped at pH 3.8 substantiated by using sizeable will increase in mild scattering intensity. At pH 2.0–2.5, WPI-PGA complexes were positively charged, and the precipitation was reduced. Therefore, pH can affect the change of the surface charge of WPI and PGA, which affects the electrostatic interaction.

Fig. 1C showed the particle size and polydispersity index (PDI) change of WPI-PGA complexes at pH 2.0–6.0. At pH 5.0–6.0, there were no interactions between WPI and PGA and the solution was transparent, with a mean particle size of 500–600 nm. Subsequently, the mean particle size of the complexes extended barely as the system was acidified, due to the increase in electrostatic interactions between WPI and PGA. Meanwhile, the overall PDI of the WPI-PGA complex was below 0.5. Which indicated that the complex was dispersed uniformly. At pH 4.0, a soluble uniform complex was formed, and the mean particle size was about 636 nm. The solution produced an insoluble coacervate and the mean particle size also increased notably when the pH dropped to 3.5. At pH 3.0, the net charge of the complex was 0, and the particle size reached its maximum of 1930 nm, and the PDI reaches a maximum of 0.837. This is steady with the giant quantities of insoluble complexes shaped at pH 3.0 in Fig. 1B. The mean particle size decreased as the pH decreased, due to the disassociation of the insoluble coacervates

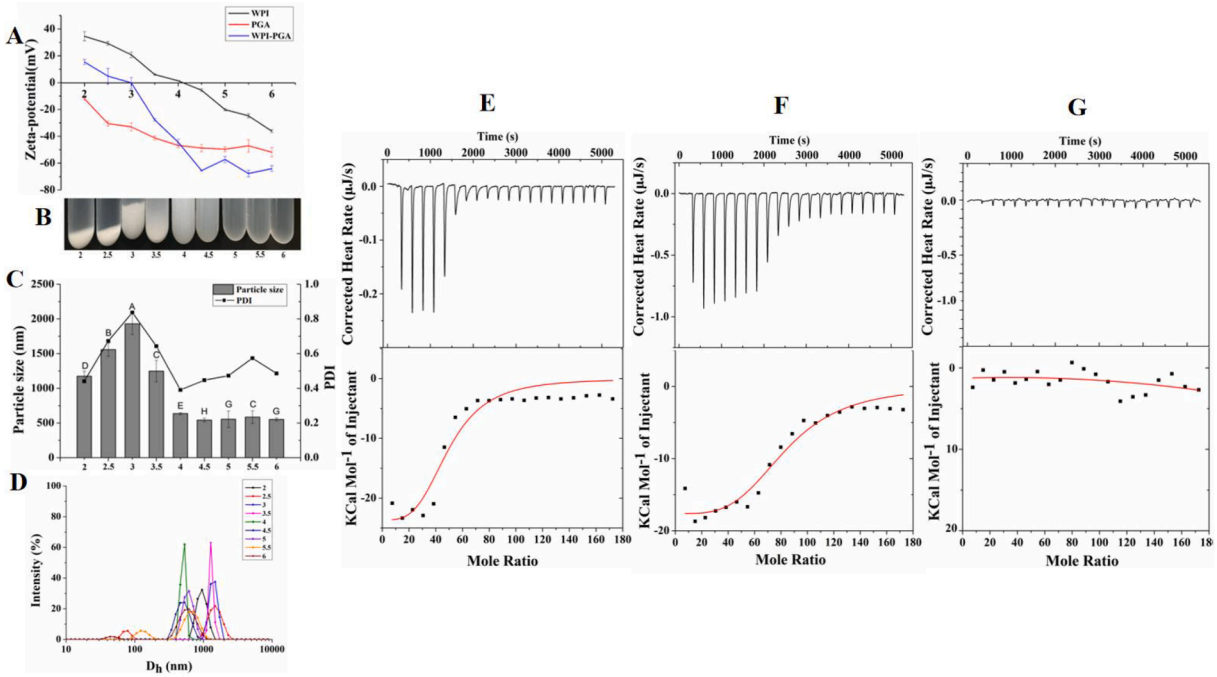

Fig. 1. Zeta potential (A), Images (B), Particle size and PDI (C) and Particle size distribution (D) of WPI-PGA complexes (total biopolymer concentration:0.6 % (w/v), R = 2:1), pH (2.0–6.0). $^{A\text{-}G}$Completely different letters in column show significant differences at $p < 0.05$. Thermograms (top panels) and binding isotherms (bottom panels) corresponding to the titration of PGA (1 μM) with WPI (500 μM) in citric acid-sodium citrate buffer solution, obtained at pH 3.5 (E), pH 4 (F) and pH 4.5 (G).

occurring between WPI and PGA with similar electrical charges.

Fig. 1D showed the changes in particle size distribution of WPI-PGA complexes at pH 2.0–6.0. At pH 5.5 and 6.0, the particle size distribution of the complexes showed a bimodal distribution, it is mainly because WPI and PGA had the same charge, and the degree of interaction was not obvious, so there were particles with different particle sizes in the solution. The complexes showed a unimodal distribution at pH 4.5, indicating that WPI and PGA began to interact locally, the particles in the solution began to aggregate, and the particle size in the solution tended to be uniform. Continuing to lower the pH, the degree of unimodal distribution of the complexes narrowed at pH 3.5 and 4.0, mainly because the electrostatic interaction of WPI and PGA was enhanced, and the complexes could be uniformly dispersed in the solution, so the particle size range in the solution decreased. The complexes show a broadened unimodal distribution at pH 3.0, indicating that strong electrostatic interactions caused the particles aggregate and form large particles, resulting in non-uniform particle size in solution, which is consistent with the appearance of precipitation in solution at pH 3.0 in Fig. 1B. When the pH was lowered to 2.5, the complexes exhibited a bimodal distribution, which may be due to the electrostatic interaction at pH 2.5 was lower than that at pH 3.0, and the insoluble particles in the solution decreased, resulting in complex particles with different particle sizes in the solution. At pH 2.0, the complexes exhibited a unimodal distribution, which may be due to the continuous decrease of electrostatic interaction, which further reduced the insoluble particles in the solution and made the particle size of the complexes tend to be uniform. Such results suggested that the effect of pH on properties of complexes may result in the mutual transformation of the monomodal particle size distribution and multimodal particle size distribution for a complex solution (Peng et al., 2022).

3.2. Effects of pH on ITC of WPI-PGA complex

ITC is a biophysical technique used in molecular biology and other fields to study molecular interactions. Despite its limitations, ITC is viewed as the gold standard for measuring biomolecular interactions (Bou-Abdallah & Terpstra, 2012). The heat flow and time relationship curves (top panel) and binding isotherm (bottom panel) were obtained between WPI (500 μM) and PGA (1 μM) at 25 ℃ and at pH 3.5, 4.0, and 4.5, respectively, as shown in Fig. 1D, E, and F. At pH 3.5 and 4.0, the interactions between WPI and PGA released energy throughout the process, which indicated this was an exothermic process. At pH 4.5, there was little change in the heat flow curve, which indicated the occurrence of a slight exothermic process between WPI and PGA. This process is typically associated with neutralization of the charge between two biopolymers with opposite charges, and it mainly depends on a change in enthalpy (ΔH) during the complex aggregation process of proteins and polysaccharides (Yang, et al., 2020). This process is explained in detail in the section on thermodynamic parameters. During the entire injection process, the exothermic curves of pH 3.5 and 4.0 stabilized after the 7th and 11th times, respectively. This result agrees with that of the ITC test conducted by Xiong et al., which showed that ovalbumin and chitosan continued to release heat during the injection process under different salt ion conditions and eventually tended to a thermodynamically stable state., which also showed that WPI and PGA The titration process is an exothermic electrostatic neutralization process (Xiong, Ren, Tian, Yang, Li, & Li, 2017). A sigmoidal curve was then fitted for the titration heat against the ratio of the ligand to the binding partner in the ITC reaction cell at pH 3.5 and 4.0. The results showed significant attenuation of the exothermic curve at pH 4.5 throughout the titration process, which occurred due to the weaker interactions between WPI and PGA when they had similar negative electrical charges at pH 4.5.

The thermodynamic parameters of the interactions between WPI and PGA were calculated, including the binding stoichiometry (N), affinity constant (K), enthalpy (ΔH), entropy contribution (ΔS), and the Gibbs free energy (ΔG) changes. As shown in Table 1, the Gibbs free energy (ΔG) of WPI-PGA complexes with different pH was negative throughout, which indicated that the binding behavior of WPI and PGA at pH 3.5 and 4.0) was a spontaneous process. The enthalpy (ΔH) contribution is related to the electrostatic interaction of the opposite charges carried by the two biopolymers (Hosseini et al., 2013). The results also showed that the binding process of WPI and PGA at pH 3.5 and 4.0 was mainly driven by enthalpy (ΔH), at -28.92 ± 7.07 kJ/mol and -21.69 ± 2.38 kJ/mol, respectively. This follows the results of dynamic light scattering and the zeta potential, which showed that WPI and PGA had opposite charges at pH 3.5 and 4.0, respectively. In this respect, the electrostatic interactions occurred due to the opposite charges. The results also indicated that the electrostatic interactions played a key role in the binding process of WPI-PGA (Chung, Kim, Cho, Ko, Hwang, & Kim, 2007). At pH 4.5, the electrostatic interactions were weak because the negative charges of WPI and PGA were the same. As this was non-resolvable within the sensitivity of our ITC instrument and the deviation of the thermodynamic parameter data was large, so the thermodynamic parameter data are not shown.

The entropy (ΔS) value reflects changes in the order of the system, and a large positive entropy value is usually due to a change in hydration when the protein and ligand are combined (Bjelic & Jelesarov, 2008). Moreover, Table 1 showed that TΔS was an important indicator affecting the binding process of WPI and PGA at pH 3.5 and 4.0 (1.54 ± 0.68 kJ/mol and 7.48 ± 1.34 kJ/mol, respectively). The positive value of entropy (ΔS) showed that it was beneficial in the whole binding process of WPI and PGA. These results are consistent with those of many previous studies, which have shown that the interaction between oppositely charged proteins and polysaccharides is driven by entropy (ΔS) and originating from the release of water molecules and counterions (de Kruif, Weinbreck, & de Vries, 2004; de Vries & Stuart, 2006). However, this result differs from that in the study of Yang et al. (Yang, et al., 2020), who considered that the unfavorable entropy (ΔS) contribution may be due to loss of macromolecule mobility after complexation, and that the main driving force depends on enthalpy entropy compensation (Aberkane, Jasniewski, Gaiani, Scher, & Sanchez, 2010). Nevertheless, the positive value of the entropy (ΔS) contribution was found to be a beneficial index in the binding process of WPI and PGA in this study.

When verifying of the titration process, the smaller thermodynamic N ratio was found to indicate the occurrence of strong interactions between the WPI-PGA copolymer complex that were beneficial for the formation of the copolymer during the complexation process. Table 1 shows that N ratio gradually increased with a decrease in pH. K showed a similar trend, and was approximately double the value of pH 4.0 at pH 3.5, which indicated strong electrostatic attraction between WPI and PGA at the same molar ratio under the conditions of pH 3.5. As excessively strong electrostatic attraction would produce large particles and insoluble coacervates, they are not conducive for analyzing particles in solution. Therefore, we selected pH 4.0 as the condition for further study.

Table 1
Thermodynamic parameters of binding between WPI and PGA at pH 3.5 and 4.0, respectively.

Samples	N	K (M^{-1})	ΔH (kJ/mol)	TΔS (kJ/mol)	ΔG (kJ/mol)
WPI-$PGA_{3.5}$	47.55 ± 7.07	(2.17 ± 0.26) × 10^5	−28.92 ± 7.07	1.54 ± 0.68	−30.46
WPI-$PGA_{4.0}$	79.50 ± 5.75	(1.29 ± 0.17) × 10^5	−21.69 ± 2.38	7.48 ± 1.34	−29.16
WPI-$PGA_{4.5}$	254.1 ± 7.27	(1.28 ± 0.32) × 10^3	−14.73 ± 1.47	3.01 ± 1.62	−17.74

3.3. Effects of pH on the fluorescence intensity of WPI-PGA complex

The local changes caused by the environmental impact of proteins can cause high sensitivity to tryptophan (Trp) (Jia, Gao, Hao, & Tang, 2017). Therefore, Trp fluorescence analysis is often used to evaluate the changes in the secondary structure of proteins relating to the interactions between biopolymers (Souza, Goncalves, & Gomez, 2011). As shown in Fig. 2A, the fluorescence intensity of the complexes increased and then decreased as the pH decreased. At pH 5.0–6.0, WPI and PGA generated electrostatic repulsion due to their similar negative electrical charges: PGA did not therefore affect the structure of WPI and the fluorescence intensity was low. At pH 4.0–4.5, the fluorescence intensity increased significantly due to the interactions between WPI and PGA, which altered the secondary structure of WPI and loosened it; this exposed more tryptophan and a gradual increase in the fluorescence intensity. The fluorescence intensity reached its maximum at pH 4.0, which indicated an increase in the electrostatic interactions between WPI and PGA and a loosening of the WPI structure. At pH lower than 2.0–3.5, WPI and PGA formed an insoluble coacervate, which led to protein aggregation with tryptophan residues in WPI hidden inside, which led to the fluorescence intensity decrease (Peinado, Lesmes, Andres, & McClements, 2010).

3.4. Effects of pH on the CD spectrum of WPI-PGA complex

CD is widely viewed as an effective technique for use in evaluating and determining the secondary structure of proteins (Kayitmazer, Seeman, Minsky, Dubin, & Xu, 2013). In this study, the CD spectra were used to evaluate the influence of PGA addition on the structural changes of WPI. As shown in Fig. 2B, the secondary structure of WPI changed as the pH changed, which indicated differences in the coacervation behavior of WPI and PGA under different pH conditions.

The secondary structure contents of the WPI in the WPI-PGA complexes at R = 2:1, with different pH values are presented in Table 2. When the pH was adjusted to 2.0–3.5, precipitation occurred in the complex solution due to strong electrostatic attraction, which lowered the concentration of the complex in the solution; therefore, a weak CD spectrum was hardly observed. Compared with pH 4.5–6.0, the α-helix structure increased to 71.1 %, and the β-sheet structure decreased to 5.4 % at pH 4.0 (Table 2). However, β-sheets are usually found in aggregated proteins, as reported in a previous study (Guerrero, Kerry, & de la Caba, 2014), and it is thus evident that conformational relaxation occurred following the interactions between WPI and PGA. This result agrees with that of the significant increase in the fluorescence intensity of WPI-PGA complex at pH 4.0, and it shows that pH affected the electrostatic interactions between WPI and PGA and changed the secondary structure of WPI.

3.5. Effects of the mass ratio on the associative coacervation behavior of WPI and PGA

Mass ratio is an important indicator affecting the interactions between WPI and PGA. Information about the mean particle size and T of WPI-PGA at pH 4.0 with different mass ratios is provided in Fig. 3A. The mean particle size of WPI was 535 nm, whereas PGA was 838 nm. In addition, the mean particle size of the WPI-PGA complexes first increased, then decreased with added PGA, and the measured polydispersity index (PDI) (Fig. 3C) of the complexes also showed a similar trend. Therefore, the mean particle size of the WPI-PGA complexes was related to the amount of PGA added. This is consistent with the phenomenon shown in Fig. 3B, where the WPI-PGA complexes are shown to change from turbid to clear under different mass ratios. The mean particle size reached a micron-level, and the turbidity increased at a mass ratio of 20:1, which indicated formation of large-particle complexes (as shown in Fig. 3B) and corresponded with the formation of micron-sized particles.

In Fig. 1A, the isoelectric point (pI) of WPI is 4.2, and according to the results of Harnsilawat et al. (2006) (Harnsilawat, Pongsawatmanit, & McClements, 2006), the dissociation constant (pKa) of PGA is 3.5. At pH 4.0, WPI and PGA had opposite electrical charges and formed a complex due to electrostatic attraction. A low PGA content caused a large mean particle size in relation to WPI coacervation. With an increase in PGA, the mean particle size of the WPI-PGA complex exhibited a decreasing trend with decreased turbidity, which showed that the addition of PGA reduced the polymerization of WPI. At a mass ratio of 2:1, the particle size of the complex was in the order of nanometers, which indicated that a small particle complex was formed. This depended on the negatively electrical charged PGA around WPI increased when enough PGA was added. In addition, the electrostatic repulsion between the WPI-PGA complexes increased, which weakened the coacervation of WPI, thus forming smaller nanoparticles. When a greater amount of PGA was added, there were no significant changes in the mean sizes of the particles in the complex, and this indicated that the interaction between WPI and PGA was close to saturation, WPI and PGA had reached their maximum binding capacity, and the charges could not be detected (Bokkhim, Bansal, Grondahl, & Bhandari, 2015).

The electrical charge characteristics of the WPI-PGA complexes at pH 4.0 with different mass ratio values are shown in Fig. 3D. The zeta potential of WPI was +12.1 mV, and the PGA was −76.8 mV. The zeta potential dropped to 11 mV when WPI and PGA were combined with a mass ratio value of 20:1, which indicated that the change was related to electrostatic attraction, and the positive and negative electrical charges were neutralized to form large-particle complexes after adding PGA. The net charge of the complex tended to 0 and the positive and negative electrical charges were neutralized when the mass ratio was 10:1. With the greater addition of PGA, the overall complex exhibited a net negative charge and the absolute value of its potential gradually increased, which

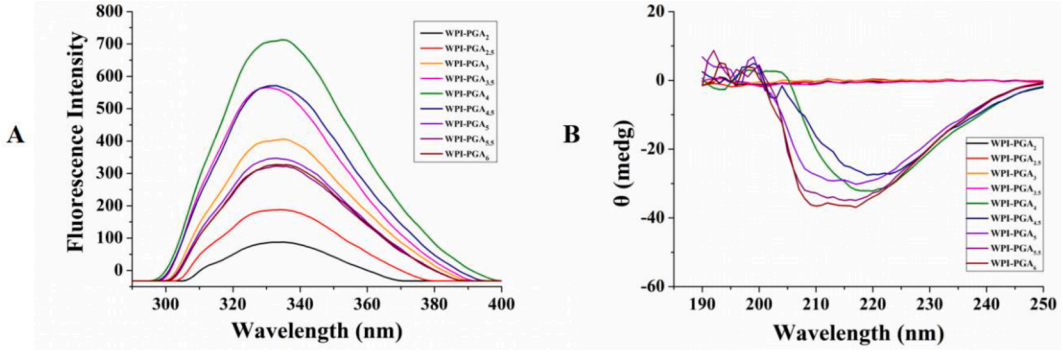

Fig. 2. Fuorescence intensity (A) of WPI-PGA complexes (total biopolymer concentration:0.6 % (w/v), R = 2:1), pH (2.0–6.0). Circular dichroism (B) of WPI-PGA complexes (total biopolymer concentration:0.6 % (w/v), R = 2:1), pH (2.0–6.0).

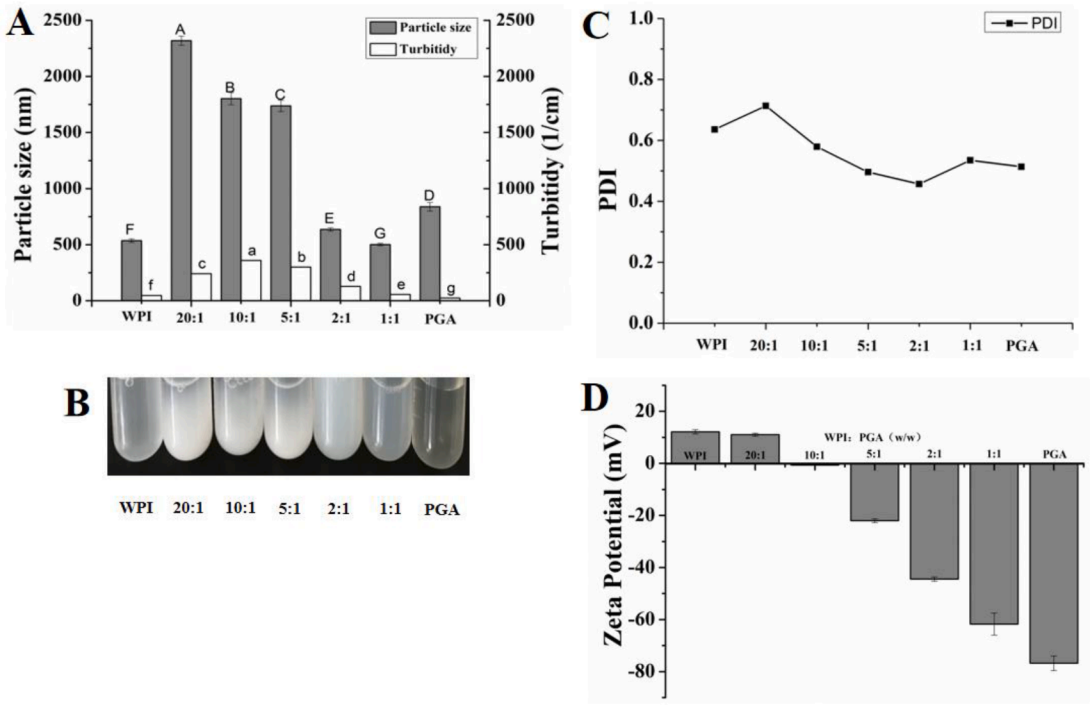

Fig. 3. Particle size and turbidity (A), Images (B), PDI (C) and Zeta potential (D) of WPI, PGA, WPI-PGA complexes with different mass ratios (20:1, 10:1, 5:1, 2:1, 1:1) at pH 4.0.

indicated that the total charge of the complex was mainly controlled by anionic PGA. A previous study reported similar phenomenon, which was explained by the outer pectin layer determining the charge characteristics of the entire biopolymer particle (Chen, Li, Ding, & Suo, 2012).

3.6. *Effects of the mass ratio on the fluorescence intensity of the WPI-PGA complex*

The conformational changes of proteins were monitored by detecting

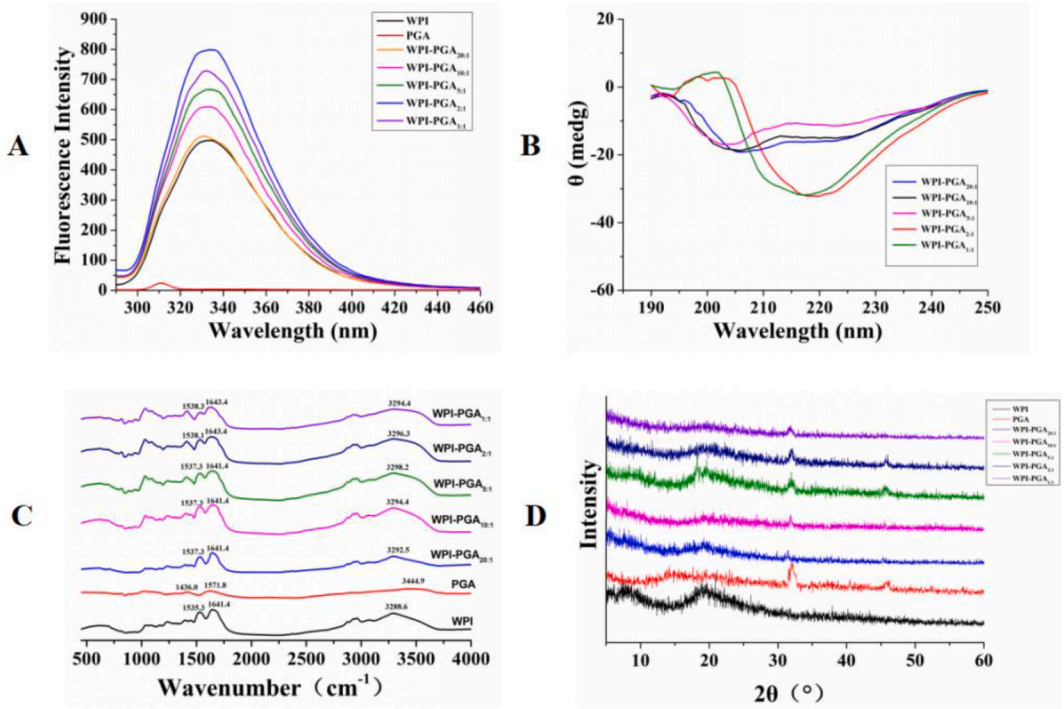

Fig. 4. Fuorescence intensity (A) of WPI, PGA and WPI-PGA complexes with different mass ratios (20:1, 10:1, 5:1, 2:1, 1:1) at pH 4.0, total biopolymer concentration:0.6% (w/v). Circular dichroism (B) of WPI-PGA complexes with different mass ratios (20:1, 10:1, 5:1, 2:1, 1:1) at pH 4.0, total biopolymer concentration:0.6% (w/v). FTIR (C) of WPI, PGA and WPI-PGA complexes with different mass ratios (20:1, 10:1, 5:1, 2:1, 1:1) at pH 4.0, total biopolymer concentration:0.6% (w/v). X-ray diffractometry (D) of WPI, PGA and WPI-PGA complexes with different mass ratios (20:1, 10:1, 5:1, 2:1, 1:1) at pH 4.0, total biopolymer concentration: 0.6% (w/v).

the fluorescence characteristics of tryptophan (Trp) in WPI-PGA with different R values. As shown in Fig. 4A, the fluorescence intensity of the WPI-PGA complexes first increased and then decreased as the mass ratio increased, and the fluorescence intensity of the complexes was stronger than for WPI alone. This occurred due to the interactions between WPI and PGA, which resulted in the following when PGA was added: the unfolding of the WPI structure, a greater amount of Trp being exposed, and an increase in the fluorescence intensity (Borges, Campina, Souza, Goncalves, & Fernando Silva, 2012). The fluorescence intensity reached a maximum at a mass ratio of 2:1 for WPI-PGA. However, an increase in the amount of PGA added caused a slight decrease in the fluorescence intensity, because excessive PGA was attached to the surface of WPI, which masked the binding site of WPI and hid the Trp, thus resulting in a decrease in fluorescence intensity (Xi, Kang, Zhao, Liu, Sun, & Zhang, 2020).

3.7. Effects of the mass ratio on the CD spectrum of the WPI-PGA complex

The CD spectrum of WPI-PGA complexes with different mass ratio values are shown in Fig. 4B. The secondary structure content of WPI was calculated using the SELCON3 mode (Table 3). When the mass ratio was 20:1 or 10:1, the α-helix decreased to 21.2 % and 41.8 %, and the β-sheet increased significantly by 23.5 % and 15 %, respectively. These results indicated that aggregation of WPI increased when the mass ratio was large, and they are consistent with those of the mean particle size shown in Fig. 5B. The results are also consistent with those of Xu et al. (2015), who showed that the percentage of protein α-helix structure was significantly reduced and that of β-sheets increased after the interaction between β-lactoglobulin and pectin. It has also been reported that β-sheets usually appear in aggregated proteins (Xu, Melton, Jameson, Williams, & McGillivray, 2015). Furthermore, it was reported that β-sheets usually appear in aggregated proteins (Lefevre & Subirade, 2000). These results prove that low concentrations of PGA helped to form aggregated WPI.

When the mass ratio was 2:1, the α-helix notably increased to 71.1 % and the β-sheet decreased to 5.4 %. This indicated that the interaction between WPI and PGA was enhanced with the increase of WPI, and the structure of WPI loosened, which agrees with the fluorescence spectroscopy results. Similar to our results, the study of (Sun, Dai, & Gao, 2017) showed that the interaction between zein and PGA at a mass ratio of 2:1 or 1:1 caused an increase in the α-helix structure and a decrease in the β-sheet structure. In summary, different mass ratios of the reactants resulted in different degrees of interactions and differences in the secondary structure of WPI.

3.8. Effects of the mass ratio on FITR of the WPI-PGA complex

FTIR can be applied to analyze changes in the interaction between biopolymers and it is often used to analyze changes in protein structure and molecular bonding. In Fig. 4C, WPI exhibited characteristic peaks at 1641.4 cm^{-1} and 1535.3 cm^{-1}, indicating the amide I band (1600–1700 cm^{-1}) and the amide II band (1450–1600 cm^{-1}), respectively. The amide I band is attributed to the stretching vibration of C—O and C—N (Pereira, Souza, Cerqueira, Teixeira, & Vicente, 2010), and the amide II band is attributed to the bending vibration of N—H and the stretching vibration of C—N (Hoque, Benjakul, & Prodpran, 2011). The PGA exhibited broad peaks around 3444.9 cm^{-1}, which represented O—H

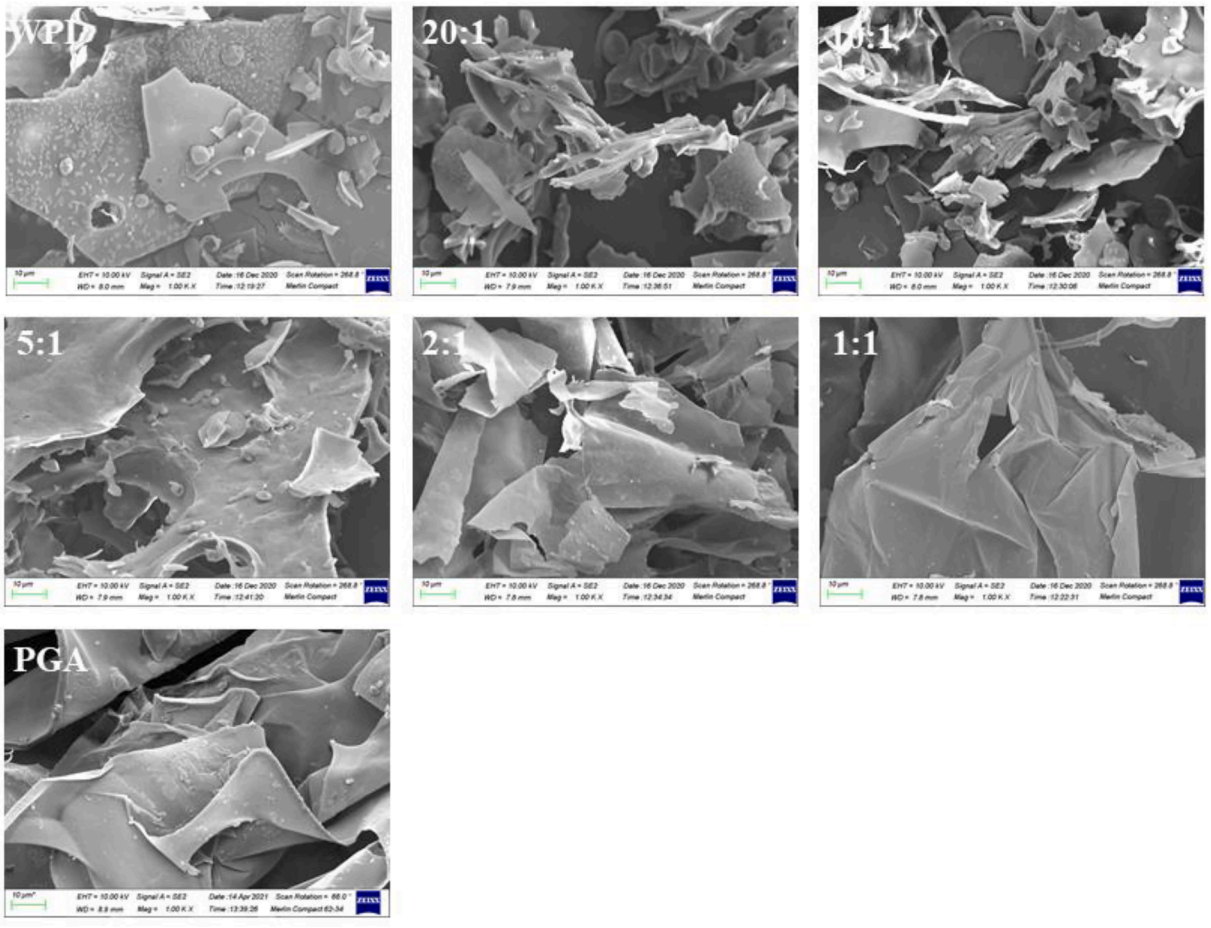

Fig. 5. SEM images of WPI, PGA and WPI-PGA complexes with different mass ratios (20:1, 10:1, 5:1, 2:1, 1:1) at pH 4.0, total biopolymer concentration:0.6% (w/v).

stretching vibration in the wavenumber range from 3500 cm^{-1} to 3000 cm^{-1}. Another characteristic peak was observed at approximately 1571.8 cm^{-1} in the PGA spectra, which corresponded to the C—O stretching vibration in the carboxyl and ester groups of PGA (Wei et al., 2019).

Litvinov et al. reported an increase in the β-sheet content of the protein secondary structure increased when the characteristic peak shifted from 1550 cm^{-1} to a low band (Litvinov, Faizullin, Zuev, & Weisel, 2012). In this study, the amide II band of the complex at the mass ratio of 2:1 shifted to a high band with an increase of the R value, from 1535.3 cm^{-1} to 1538.3 cm^{-1}; therefore, the β-sheet was reduced in the secondary structure of WPI at the mass ratio of 2:1 (Guerrero, Kerry, & de la Caba, 2014). This agrees with the results of the CD spectrum, where the WPI structure unfolded due to electrostatic interactions, the structure of WPI unfolded, and the electrostatic interactions increased as mass ratio increased. In addition, the stretching vibration of the hydroxyl group at approximately 3290 cm^{-1} was a manifestation of hydrogen (H) bond enhancement (Zou, Mourad, Zhang, Ahn, Cai, & Jin, 2020), and the interactions between WPI and PGA shifted the peak of WPI at 3288 cm^{-1}, thus enhancing the hydrogen bond in the structure. These results indicated that hydrogen bonding was also one of the interaction forces involved.

3.9. Effects of the mass ratio on the XRD of the WPI-PGA complex

XRD is a method used to observe whether the structural characteristics of samples are crystalline or amorphous, and it was also used here to explain the structural changes after the interactions between WPI and PGA. The 2θ angles of the diffraction peaks of WPI were 7.84° and 19.7°, as shown in Fig. 4D, and the main diffraction peaks of PGA were 7.24° and 16.6°. The diffractograms of WPI and PGA showed broad and slow peaks, which indicated that the two substances were in an amorphous structural state. The shapes of the peak spectrum in the WPI-PGA diffraction patterns at several mass ratio values showed that WPI and PGA retained an amorphous structure, but the peak intensity was reduced. This indicated that the amorphous structure of WPI-PGA complexes increased compared to their singular structures, and it confirmed the intermolecular interactions between WPI and PGA. These results agree with those of a previous study that investigated the formation of the uniform and amorphous structure of WPI-tamarind seed mucilage (Gonzalez-Martinez, Carrillo-Navas, Barrera-Diaz, Martinez-Vargas, Alvarez-Ramirez, & Perez-Alonso, 2017).

3.10. Effects of the mass ratio on the SEM of the WPI-PGA complex

The freeze-dried surface morphology of WPI and PGA with different mass ratios values was captured using SEM. As shown in the Fig. 5, WPI was more evenly distributed and had a sheet-like structure, but the surface and shape of the binary complexes changed with the addition of PGA. The WPI-PGA had a clump structure at mass ratios of 20:1 and 10:1, and the surfaces of the complexes were rough and the particle diameters large. These results agree with those of dynamic light scattering. When PGA was increasingly added, the interactions between WPI and PGA formed a small particle complex, the cluster structure gradually dissociated, and it was restored to the original lamellar structure and became uniform. The complexes exhibited a filamentous structure when PGA was added at a mass ratio of 1:1.

4. Conclusions

In this study, pH was the major factor affecting changes in the thermodynamic parameters under the same molar ratio through the ITC test, enthalpy (ΔH) and the positive value of entropy (ΔS) contribution were the beneficial index in the binding process of WPI and PGA. FTIR confirmed that hydrogen bonding was also one of the interaction forces besides the electrostatic interactions between the uniform complex formed by WPI and PGA. Fluorescence spectroscopy and CD showed that adding PGA unfolded the secondary structure of WPI, leading to more exposure of Trp residues in WPI. XRD and SEM showed the amorphous structures of freeze-dried WPI-PGA complexes were more significant and formed a smoother and uniform structure. Therefore, we provided a theoretical basis for the non-covalent interaction mechanism of WPI and PGA, studied the structural characteristics and physicochemical indicators of the WPI-PGA electrostatic complex and provided insights for further applied research in the future.

CRediT authorship contribution statement

Chunyu Xi: Conceptualization, Validation, Supervision, Writing – review & editing. **Zhengwei Sun:** Conceptualization, Investigation, Data curation, Formal analysis, Writing – original draft, Writing – review & editing. **Xing Chen:** Data curation, Investigation, Supervision, Validation. **Xuan Ding:** Data curation, Validation. **Tiehua Zhang:** Conceptualization, Validation, Supervision, Writing – review & editing.

Declaration of Competing Interest

The authors declare that they have no known competing financial interests or personal relationships that could have appeared to influence the work reported in this paper.

Acknowledgements

We acknowledge the financial support from the Science and Technology Program of Jilin Province (3D5204222430). We also thank Editage (www.editage.cn) for the English language editing.

Appendix A. Supplementary data

Supplementary data to this article can be found online at https://doi.org/10.1016/j.fochx.2022.100402.

References

Aberkane, L., Jasniewski, J., Gaiani, C., Scher, J., & Sanchez, C. (2010). Thermodynamic characterization of acacia gum-beta-lactoglobulin complex coacervation. *Langmuir, 26*(15), 12523–12533.

Azeredo, H. M. C., & Waldron, K. W. (2016). Crosslinking in polysaccharide and protein films and coatings for food contact - A review. *Trends in Food Science & Technology, 52*, 109–122.

Bjelic, S., & Jelesarov, I. (2008). A survey of the year 2007 literature on applications of isothermal titration calorimetry. *Journal of Molecular Recognition, 21*(5), 289–311.

Bokkhim, H., Bansal, N., Grondahl, L., & Bhandari, B. (2015). Interactions between different forms of bovine lactoferrin and sodium alginate affect the properties of their mixtures. *Food Hydrocolloids, 48*, 38–46.

Borges, J., Campina, J. M., Souza, H. K. S., Goncalves, M. P., & Fernando Silva, A. (2012). Aggregation-induced conformational transitions in bovine beta-lactoglobulin adsorbed onto open chitosan structures. *Soft Matter, 8*(4), 1190–1201.

Bou-Abdallah, F., & Terpstra, T. R. (2012). The thermodynamic and binding properties of the transferrins as studied by isothermal titration calorimetry. *Biochimica Et Biophysica Acta-General Subjects, 1820*(3), 318–325.

Chen, B., Li, H., Ding, Y., & Suo, H. (2012). Formation and microstructural characterization of whey protein isolate/beet pectin coacervations by laccase catalyzed cross-linking. *LWT-Food Science and Technology, 47*(1), 31–38.

Chung, K., Kim, J., Cho, B.-K., Ko, B.-J., Hwang, B.-Y., & Kim, B.-G. (2007). How does dextran sulfate prevent heat induced aggregation of protein?: The mechanism and its limitation as aggregation inhibitor. *Biochimica Et Biophysica Acta-Proteins and Proteomics, 1774*(2), 249–257.

de Kruif, C. G., Weinbreck, F., & de Vries, R. (2004). Complex coacervation of proteins and anionic polysaccharides. *Current Opinion in Colloid & Interface Science, 9*(5), 340–349.

de Vries, R., & Stuart, M. C. (2006). Theory and simulations of macroion complexation. *Current Opinion in Colloid & Interface Science, 11*(5), 295–301.

Doost, A. S., Nasrabadi, M. N., Kassozi, V., Dewettinck, K., Stevens, C. V., & Van der Meeren, P. (2019). Pickering stabilization of thymol through green emulsification using soluble fraction of almond gum - Whey protein isolate nano-complexes. *Food Hydrocolloids, 88*, 218–227.

Feng, S., Sun, Y., Wang, D., Sun, P., & Shao, P. (2020). Effect of adjusting pH and chondroitin sulfate on the formation of curcumin-zein nanoparticles: Synthesis, characterization and morphology. *Carbohydrate Polymers, 250*.

Gonzalez-Martinez, D. A., Carrillo-Navas, H., Barrera-Diaz, C. E., Martinez-Vargas, S. L., Alvarez-Ramirez, J., & Perez-Alonso, C. (2017). Characterization of a novel complex coacervate based on whey protein isolate-tamarind seed mucilage. *Food Hydrocolloids, 72*, 115–126.

Gorji, S. G., Gorji, E. G., & Mohammadifar, M. A. (2014). Characterisation of gum tragacanth (Astragalus gossypinus)/sodium caseinate complex coacervation as a function of pH in an aqueous medium. *Food Hydrocolloids, 34*(1), 161–168.

Guerrero, P., Kerry, J. P., & de la Caba, K. (2014). FTIR characterization of protein-polysaccharide interactions in extruded blends. *Carbohydrate Polymers, 111*, 598–605.

Guo, B., Hu, X., Wu, J., Chen, R., Dai, T., Liu, Y., … Liu, C. (2021). Soluble starch/whey protein isolate complex-stabilized high internal phase emulsion: Interaction and stability. *Food Hydrocolloids, 111*.

Harnsilawat, T., Pongsawatmanit, R., & McClements, D. J. (2006). Characterization of beta-lactoglobulin-sodium alginate interactions in aqueous solutions: A calorimetry, light scattering, electrophoretic mobility and solubility study. *Food Hydrocolloids, 20*(5), 577–585.

Hoque, M. S., Benjakul, S., & Prodpran, T. (2011). Effects of partial hydrolysis and plasticizer content on the properties of film from cuttlefish (Sepia pharaonis) skin gelatin. *Food Hydrocolloids, 25*(1), 82–90.

Hosseini, S. M. H., Emam-Djomeh, Z., Razavi, S. H., Moosavi-Movahedi, A. A., Saboury, A. A., Mohammadifar, M. A., … Van der Meeren, P. (2013). Complex coacervation of beta-lactoglobulin - kappa-Carrageenan aqueous mixtures as affected by polysaccharide sonication. *Food Chemistry, 141*(1), 215–222.

Jia, J., Gao, X., Hao, M., & Tang, L. (2017). Comparison of binding interaction between beta-lactoglobulin and three common polyphenols using multi-spectroscopy and modeling methods. *Food Chemistry, 228*, 143–151.

Kayitmazer, A. B., Seeman, D., Minsky, B. B., Dubin, P. L., & Xu, Y. (2013). Protein-polyelectrolyte interactions. *Soft Matter, 9*(9), 2553–2583.

Klein, M., Aserin, A., Ben Ishai, P., & Garti, N. (2010). Interactions between whey protein isolate and gum Arabic. *Colloids and Surfaces B-Biointerfaces, 79*(2), 377–383.

Kuhn, K. R., Drummond e Silva, F. G., Netto, F. M., & da Cunha, R. L. (2014). Assessing the potential of flaxseed protein as an emulsifier combined with whey protein isolate. *Food Research International, 58*, 89–97.

Lefevre, T., & Subirade, M. (2000). Molecular differences in the formation and structure of fine-stranded and particulate beta-lactoglobulin gels. *Biopolymers, 54*(7), 578–586.

Litvinov, R. I., Faizullin, D. A., Zuev, Y. F., & Weisel, J. W. (2012). The alpha-helix to beta-sheet transition in stretched and compressed hydrated fibrin clots. *Biophysical Journal, 103*(5), 1020–1027.

Liu, J., Shim, Y. Y., Shen, J., Wang, Y., & Reaney, M. J. T. (2017). Whey protein isolate and flaxseed (Linum usitatissimum L.) gum electrostatic coacervates: Turbidity and rheology. *Food Hydrocolloids, 64*, 18–27.

Peinado, I., Lesmes, U., Andres, A., & McClements, D. J. (2010). Fabrication and morphological characterization of biopolymer particles formed by electrostatic complexation of heat treated lactoferrin and anionic polysaccharides. *Langmuir, 26*(12), 9827–9834.

Peng, B., Li, Z., Xiong, Q., Wu, C., Huang, J., Zhou, R., & Jin, Y. (2022). Casein-dextran complexes subjected to microfiltration: Colloidal properties and their corresponding processing behaviors. *Journal of Food Engineering, 320*.

Pereira, R. N., Souza, B. W. S., Cerqueira, M. A., Teixeira, J. A., & Vicente, A. A. (2010). Effects of electric fields on protein unfolding and aggregation: Influence on edible films formation. *Biomacromolecules, 11*(11), 2912–2918.

Samanta, R., & Ganesan, V. (2018). Influence of protein charge patches on the structure of protein-polyelectrolyte complexes. *Soft Matter, 14*(46), 9475–9488.

Schmitt, C., & Turgeon, S. L. (2011). Protein/polysaccharide complexes and coacervates in food systems. *Advances in Colloid and Interface Science, 167*(1–2), 63–70.

Shang, J., Liao, M., Jin, R., Teng, X., Li, H., Xu, Y., … Liu, N. (2021). Molecular properties of Flammulina velutipes Polysaccharide-Whey Protein Isolate (WPI) complexes via noncovalent interactions. *Foods, 10*(1).

Shi, R., Li, T., Li, M., Munkh-Amgalan, G., Qayum, A., Bilawal, A., & Jiang, Z. (2021). Consequences of dynamic high-pressure homogenization pretreatment on the physicochemical and functional characteristics of citric acid-treated whey protein isolate. *LWT-Food Science and Technology*, 136.

Souza, H. K. S., Goncalves, M.d. P., & Gomez, J. (2011). Effect of chitosan degradation on its interaction with beta-Lactoglobulin. *Biomacromolecules, 12*(4), 1015–1023.

Sun, C., Dai, L., & Gao, Y. (2017). Interaction and formation mechanism of binary complex between zein and propylene glycol alginate. *Carbohydrate Polymers, 157*, 1638–1649.

Wei, Y., Wang, C., Liu, X., Liao, W., Zhang, L., Chen, S., … Gao, Y. (2021). Effects of microfluidization and thermal treatment on the characterization and digestion of curcumin loaded protein-polysaccharide-tea saponin complex nanoparticles. *Food & Function, 12*(3), 1192–1206.

Wei, Y., Yu, Z., Lin, K., Sun, C., Dai, L., Yang, S., … Gao, Y. (2019). Fabrication and characterization of resveratrol loaded zein-propylene glycol alginate-rhamnolipid composite nanoparticles: Physicochemical stability, formation mechanism and in vitro digestion. *Food Hydrocolloids, 95*, 336–348.

Wu, D., Lin, Q., Singh, H., & Ye, A. (2020). Complexation between whey protein and octenyl succinic anhydride (OSA)-modified starch: Formation and characteristics of soluble complexes. *Food Research International, 136*.

Xi, C., Kang, N., Zhao, C., Liu, Y., Sun, Z., & Zhang, T. (2020). Effects of pH and different sugars on the structures and emulsification properties of whey protein isolate-sugar conjugates. *Food. Bioscience, 33*.

Xiong, W., Ren, C., Jin, W., Tian, J., Wang, Y., Shah, B. R., … Li, B. (2016). Ovalbumin-chitosan complex coacervation: Phase behavior, thermodynamic and rheological properties. *Food Hydrocolloids, 61*, 895–902.

Xiong, W., Ren, C., Tian, M., Yang, X., Li, J., & Li, B. (2017). Complex coacervation of ovalbumin-carboxymethylcellulose assessed by isothermal titration calorimeter and rheology: Effect of ionic strength and charge density of polysaccharide. *Food Hydrocolloids, 73*, 41–50.

Xu, A. Y., Melton, L. D., Jameson, G. B., Williams, M. A. K., & McGillivray, D. J. (2015). Structural mechanism of complex assemblies: Characterisation of beta-lactoglobulin and pectin interactions. *Soft Matter, 11*(34), 6790–6799.

Yadav, M. P., Johnston, D. B., & Hicks, K. B. (2007). Structural characterization of corn fiber gums from coarse and fine fiber and a study of their emulsifying properties. *Journal of Agricultural and Food Chemistry, 55*(15), 6366–6371.

Yang, W., Deng, C., Xu, L., Jin, W., Zeng, J., Li, B., & Gao, Y. (2020). Protein-neutral polysaccharide nano- and micro-biopolymer complexes fabricated by lactoferrin and oat beta-glucan: Structural characteristics and molecular interaction mechanisms. *Food Research International, 132*.

Zou, W., Mourad, F. K., Zhang, X., Ahn, D. U., Cai, Z., & Jin, Y. (2020). Phase separation behavior and characterization of ovalbumin and propylene glycol alginate complex coacervates. *Food Hydrocolloids, 108*.